CrossMark

Synthesis of graphene/Fe$_3$O$_4$/NiO magnetic nanocomposites and its application in photocatalytic degradation the organic pollutants in wastewater

Guoping Zhao[1] · Zunli Mo[1] · Ping Zhang[1] · Bo Wang[1] · Xiaobo Zhu[1] · Ruibin Guo[1]

Abstract In this paper, a new type of magnetic photocatalyst graphene/Fe$_3$O$_4$/NiO (GNs/Fe$_3$O$_4$/NiO) nanocomposites have been first synthesized by a facile route. The as-prepared products have been characterized by scanning electron microscopy, Transmission electron microscope, Fourier transform infrared spectroscopy, X-ray diffraction, thermal gravimetric analysis, vibrating sample magnetometry, energy dispersive X-ray spectroscopy. The experimental results showed that magnetic GNs/Fe$_3$O$_4$/NiO nanocomposites exhibited significantly enhanced magnetic and adsorption performance, and the saturation magnetization of three kinds nanocomposites GNs/Fe$_3$O$_4$/NiO (S1), GNs/Fe$_3$O$_4$/NiO (S2) and GNs/Fe$_3$O$_4$/NiO (S3) were about 63.07, 43.33 and 22.42 emu g^{-1}, respectively. It was found that the composite materials has perfect photocatalytic performance for degrade p-nitrophenol and rhodamine B by analyzing its photocatalytic degradation performance. Moreover, the nanocomposites can be adsorbed and recycled by extra magnetic field after photocatalytic degradation of p-nitrophenol and rhodamine B in wastewater. Therefore, this kinds of magnetic nanocomposites may have great potential applications in photocatalytic field in the future.

Keywords Graphene · NiO · Magnetic nanocomposites · Photocatalytic degradation · Wastewater treatment

✉ Zunli Mo
mozlnwnu2011@163.com

[1] Key Laboratory of Eco-Environment-Related Polymer Materials, Ministry of Education of China, Key Laboratory of Polymer Materials of Gansu Province, College of Chemistry and Chemical Engineering, Northwest Normal University, Lanzhou 730070, People's Republic of China

1 Introduction

In recent years, environmental pollution is becoming more and more serious, especially the pollution of dyes to water, because the dyes are widely used in textiles, printing, dyeing, dyestuff manufacturing, and food plants, which are major sources of environmental pollution. And the pollution of dyes to water have led to an attracted extensive attention for wastewater treatment in the world. The dyes in water are commonly toxic and some of them are carcinogenic and mutagenic, resulting in adverse impact on human health [1]. Photocatalysis as a more powerful method has attractive potential applications in the degradation of toxic water pollutants [2–4]. However, so far, most photocatalytic degradation studies have focused on the utilization of nanosized metal oxide nanocomposites photocatalysts [5–8]. In the past few decades, various techniques have been developed to remove residual dyes and herbicides from contaminated media, such as biological and physical–chemical means [9, 10], either through degradation or retention [11, 12]. However, these techniques are usually not attractive due to low removal efficiency, high operation costs, secondary pollution, or time-consuming processes. Photodegradation process of dye and herbicide pollutants has attracted increasing attention during the past decades [13–15]. Among various strategies, thanks to its excellent photocatalytic effect, long-term stability and relative non-toxicity, NiO has been widely applied in photocatalytic degradation. So, NiO-based nanocomposites photocatalytic have gained special attention, such as most widely used for photodegradation of various pollutants and water purification [16]. NiO-based materials have been the most promising candidates for photocatalytic decontamination.

Graphene, a novel two-dimensional (2D) carbonaceous material with honeycomb crystal structure and atom-thick

layer features, has become a sparkling rising star on the horizon of materials science, due to its many potential applications in physical, chemical, biological, photoelectric, and catalytic fields [17–19]. Proper combination of graphene and NiO will give rise a nanocomposite hybrid material that gives desirable properties of the respective material in specific applications. Because graphene has perfect sp^2-hybridized 2D carbon structure with excellent conductivity and large surface area [20, 21], its large specific surface area increased adsorptivity [22, 23], which greatly promoted the photocatalytic removal efficiency for organic pollutants [24–26]. To date, most of the reported work focused on revealing potential excellent photocatalytic performances of the graphene-NiO nanocomposite, while little attention [27–29] has been paid to the recovery and reusability of the photocatalysts, which is crucial and decides their further practical applications. Because of the graphene-NiO nanocomposite can't be recycled and reused, the utilization rate of photocatalytic materials was very low, but Fe_3O_4 magnetic nanocomposites have attracted much attention due to its strong magnetic properties and can be separated quickly and easily in the presence of external magnetic field [30]. So, combination of the graphene nanocomposite and Fe_3O_4 nanoparticles can be recycled and reused, it improved the utilization ratio of the resources.

Herein we report a facile and fast way for the synthesis of magnetic photocatalyst $GNs/Fe_3O_4/NiO$ nanocomposites. In addition, graphene nanocomposites also can be used as adsorbent, but after combination with NiO and Fe_3O_4 magnetic particles, it has a more strong adsorption ability and good photocatalytic performance to photocatalytic degradation of p-nitrophenol and rhodamine B in wastewater. However, there are few studies concerning the effect of microstructure of magnetic constituents on magnetic absorption properties of graphene-magnetic nanomaterials. In this work, the contents of NiO and Fe_3O_4 have effected on the magnetic absorption properties and photocatalytic performance of $GNs/Fe_3O_4/NiO$ nanocomposites has been studied. The results indicated that Fe_3O_4 has significant effect on the magnetic absorbing performance of $GNs/Fe_3O_4/NiO$ nanocomposites, the content of NiO has significant effect on the photocatalytic performance of $GNs/Fe_3O_4/NiO$ nanocomposites. In the future, this kinds of the magnetic composite materials will have a wide range of applications in wastewater treatment [31].

2 Experimental

2.1 Reagents

All of the chemicals and reagents used in this study were purchased from Sinoharm Chemical Reagent Co., Ltd, China as analytical reagent grade and used without further purification. Deionized water was used in all experiments.

2.2 Experimental section

2.2.1 The preparation of graphene oxide (GO)

Graphene oxide (GO) were synthesized using natural graphite flakes by a modified Hummers method [32]. First, flake graphite (1.0 g), H_2SO_4 (35 mL) and $NaNO_3$ (1.0 g) were placed in a round bottom flask and fully cooled to 3–5 °C in an ice bath. After 15 min stirring, $KMnO_4$ (3.5 g) was slowly added over 30 min. The mixture was further stirred for 1 h at 10 °C and then heated to 35 °C. The temperature was accurately maintained at 35 °C for 2 h. After that, 35 mL H_2O was dripped into the mixture while the temperature of the reactants was kept at 95 °C for 30 min. The obtained viscous mud was diluted in 140 mL water, and then 10 mL H_2O_2 was added to reduce the unreacted oxidant until the slurry turned golden yellow. The warm solution was filtered, then washed with 5 % HCl solution and deionized water for several times. GO was finally obtained after dried in a vacuum oven at 60 °C for 24 h.

2.2.2 The preparation of graphene/Fe₃O₄ (GNs/Fe₃O₄)

The graphene/Fe_3O_4 nanocomposites [33, 34] were synthesized by a simple hydrothermal method. In a typical synthesis, 100 mg GO was dissolved in 100 mL deionized water under sonication for 60 min. Then, 6 mmol ferric citrate ($C_6H_5FeO_7$) was added into the solution and stirred at 80 °C for 1 h to guarantee a complete combination of the metal ion and the oxygen-containing functional groups on the edges and surface of GO. The resulting solution was transferred to a Teflon-line stainless steel autoclave and heated at 200 °C for 12 h. After cooling down to room temperature, the product was centrifuged and washed several times by alcohol and deionized water before drying at 60 °C for 12 h. The resulting powder was loaded into a tube furnace and heated under a continuous high-purity argon gas atmosphere from room temperature to 500 °C at a heating rate of 5 °C min^{-1} and held at this temperature for 3 h to improve the crystallinity of graphene/Fe_3O_4 nanocomposites.

2.2.3 The preparation of NiO nanoparticles

12 g $NiCl_2 \cdot 6H_2O$, 7.5 g $CO(NH_2)_2$ (precipitant) and 30 mL distilled water added into 250 mL flask, stirring 30 min to ensure completely dissolved, then heated the mixture and kept a fast stirring speed, made the solution boiling. After refluxing of 90 min, removed the flask immediately and

cooling 20 min under water, filter the sediment, washed 3 times with distilled water and obtained $Ni(OH)_2$ precipitate. Put the precipitate in the drum wind drying oven and drying 2 h at 80 °C. After dryed, put it in the muffle furnace and calcination 3 h at 550 °C, NiO nanoparticles [35] can be obtained (Fig. 1).

2.2.4 The preparation of graphene/Fe₃O₄/NiO magnetic nanocomposites

In this experiment, three kinds of nanocomposites were prepared, the content (wt%) of NiO was 50 % (S1), 67 % (S2), 75 % (S3), respectively. The resulting GNs/Fe₃O₄, NiO MNPs and 10 mg dodecyl benzene sulfonic acid sodium (SDBS) were added into 100 mL ethylene glycol and sonicated for 60 min, after being dispersed evenly, the solution was poured into a 250 mL three-necked flask, under the protection of nitrogen at room temperature and mechanical stirring for 24 h. Put the solution into a beaker, using additional magnetic field to separate the product and solution, using ethanol washed for three times, GNs/Fe₃O₄/NiO nanocomposites was obtained after vacuum dried at 60 °C.

2.3 Characterization

The surface morphology of GNs/Fe₃O₄/NiO nanocomposites were characterized by Scanning electron microscopy (SEM, JSM-6701F Japan). The microstructures of GNs/Fe₃O₄/NiO nanocomposite were characterized by X-ray diffraction (XRD, JEOL100CX). Fourier transforms infared (FT-IR) spectra of the composites in KBr pellets were recorded on an EQUINOX55 FT-IR spectrometer (Bruker). X-ray diffraction studies were performed by using D/max-2400 diffraction X-ray diffractometer (Rigaku) with Cu Kα radiation (λ = 0.154 nm) operated at 40 kV and 30 mA. The weight loss temperature of the nanocomposites was determined with a Perkin-Elmer thermogravimetric analyzer (TG–DTA; model SSC-5200) from 25 to 800 °C under nitrogen atmosphere (10 °C min⁻¹). The magnetic properties of the as-synthesized nanoparticles were measured using vibrating sample magnetometry (VSM).

2.4 Photocatalytic performance measurement

The photocatalytic activity of samples was measured by XPA-7 photocatalytic reactor (Xujiang Machine Plant, Nanjing). The temperature of the reaction was maintained at room temperature by circulating water. A 100 W medium-pressure mercury lamp was applied for a light source. First, 50 mg sample was dispersed in a 100 mL p-nitrophenol and rhodamine B aqueous solution with the initial concentration of 10 mg L⁻¹. The suspension was stirred in darkness for 30 min to reach an adsorption–desorption equilibrium. Then, turning on the light, the samples were taken from the mixture in 20 min intervals testing the photocatalytic activity. The concentration of p-nitrophenol and rhodamine B was determined at the wavelength 317 and 554 nm by UV–Vis spectrophotometer (UV-2550, Shimadzu, Japan), respectively. The degradation efficiency η (%) can be calculated as:

$$\eta = \frac{C_0 - C}{C_0} \times 100\%$$

where C_0 is the initial concentration of dye and C is the revised concentration considering dye adsorption on the catalyst after photo-irradiation.
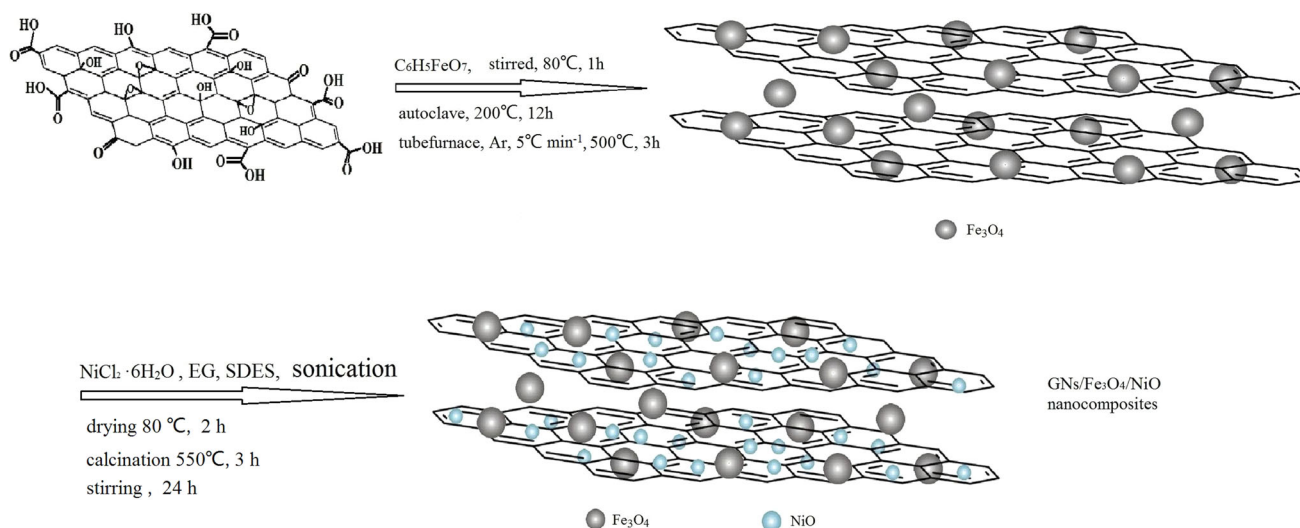

Fig. 1 Schematic illustration of the synthesis of GNs/Fe₃O₄/NiO nanocomposites

3 Results and discussion

3.1 FT-IR analysis

The FT-IR spectrum of GO (a), Fe_3O_4 MNPs (b), GNs/Fe_3O_4 (c) and GNs/Fe_3O_4/NiO (d) nanocomposites are shown in Fig. 2. The FT-IR spectrum of GO (a), the peak at 3450 cm^{-1} is due to O–H stretching vibration, the peak at 1714 cm^{-1} is due to C=O stretching vibration of carboxyl, and the peaks at 1390 and 1053 cm^{-1} are attributed to C–O stretching vibration. The peak at 1620 cm^{-1} can be assigned either to oxygen surface compounds, such as cyclic ethers, or to ring vibrations of the basal plane [36]; In the FT-IR spectrum of Fe_3O_4 MNPs (b), the vibration of Fe–O was clearly observed at 579 cm^{-1} [37]. While in the FT-IR spectrum (c) of GNs/Fe_3O_4 nanocomposites, the strong peak at 1725 cm^{-1} belonging to –C=O/–COOH vibration of GO disappears, indicating reduction of GO the Fe–O characteristic stretching vibration peak at 568 cm^{-1} was observed in curve b, which implied that Fe_3O_4 NPs was successfully anchored onto graphene sheets. Moreover, the graphene/Fe_3O_4 nanocomposite exhibited a new peak at 1564 cm^{-1} attributing to the asymmetric vibration of carboxyl, which demonstrated plenty of COO- from graphene coordinated with Fe^{3+} [37], the FT-IR spectrum of GNs/Fe_3O_4/NiO (d), peaks at $\sim$500 cm^{-1} (stretching vibration of Ni–O) and 579 cm^{-1} (vibration of Fe–O), suggesting existence of Fe_3O_4 and NiO in the nanocomposite.

3.2 SEM and TEM analysis

The surface morphology and microstructures of GNs and GNs/Fe_3O_4/NiO nanocomposite were characterized by SEM and TEM are shown in Fig. 3. Figure 3a ascribed the
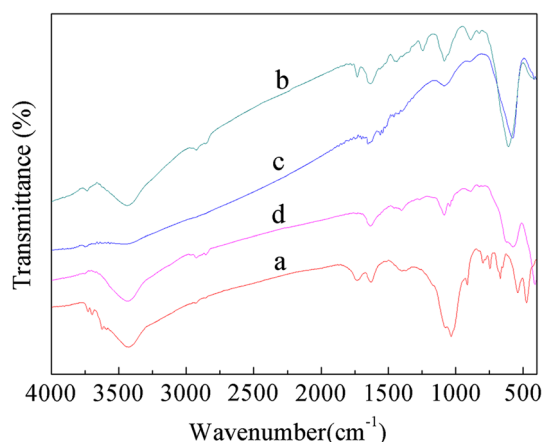

Fig. 2 The FT-IR spectrum of GO (*a*), Fe_3O_4 MNPs (*b*), GNs/Fe_3O_4 (*c*) and GNs/Fe_3O_4/NiO (*d*) nanocomposites

SEM image of GNs. In general, graphene nanosheets tend to congregate together to form multilayer agglomerates. The individual nanosheets have sizes extending from tens to several hundreds of square nanometers. The SEM of GNs/Fe_3O_4/NiO nanocomposites as shown in Fig. 3b, it showed that small NiO and Fe_3O_4 nanoparticles were uniformly embedded in the curly graphene nanosheets. The TEM image of GNs as shown in Fig. 3c. The TEM of GNs/Fe_3O_4/NiO nanocomposites as shown in Fig. 3d, the NiO and Fe_3O_4 nanoparticles are uniform in size with spherical grains which are evenly distributed on the two-dimensional graphene substrate the NiO and Fe_3O_4 nanoparticles are surrounded by flexible graphene nanosheets, which can preserve the three-dimensional structure of the GNs/Fe_3O_4/NiO nanocomposites.

To better identify the elemental composition of the synthesized composite, the elemental analysis of the composite was carried out by acquiring energy dispersive X-ray spectroscopy (EDX) spectra. One typical EDX spectroscopy for sample GNs/Fe_3O_4/NiO (S3), which is shown in Fig. 4, the results confirms the existence of Ni, Fe, C and O elements (Au peaks from spray gold on the preparation of SEM sample). In overall spectra, the C element originates from the grapheme, the Ni originates from the NiO precursor material, the Fe element originates from the Fe_3O_4, and the O element originates from GNs, Fe_3O_4 and NiO. The results in the Fig. 4 also confirms the presence of Fe in the composite with the strong peaks at 0.68 keV. The EDX element mapping analyses further identify that Fe_3O_4 and NiO MNPs were uniformly attached on the grapheme surface, which was consistent with the SEM and TEM figure.

3.3 TGA analysis

The TGA curves of GO (a), GNs (b), GNs/Fe_3O_4 (c) and Fe_3O_4/NiO/GNs (d) nanocomposites are showed in Fig. 5. As can be seen from Fig. 5, the graphite oxide had two times of quality loss in the test temperature range. At temperatures below 150 °C, quality loss is mainly causing by the volatile of water molecules, the quality loss between 200 and 300 °C, it may be due to the thermal decomposition of containing oxygen groups of graphite oxide, and the formation CO, CO_2, H_2O and so on [38]. When the graphite oxide was reduced to graphene (b), mild loss of quality in the temperature range of 150 °C within, is caused by the volatile of a small amount adsorbed water; in the temperature range of 150–800 °C within, mass loss is not obviously decreased. It shows that after graphite oxide was reduced to the graphene, most containing oxygen groups has been removed after graphite oxide was reduced to the graphene. The graphene has very good thermal stability. Figure 5c shows the TGA curves of GNs/Fe_3O_4, it
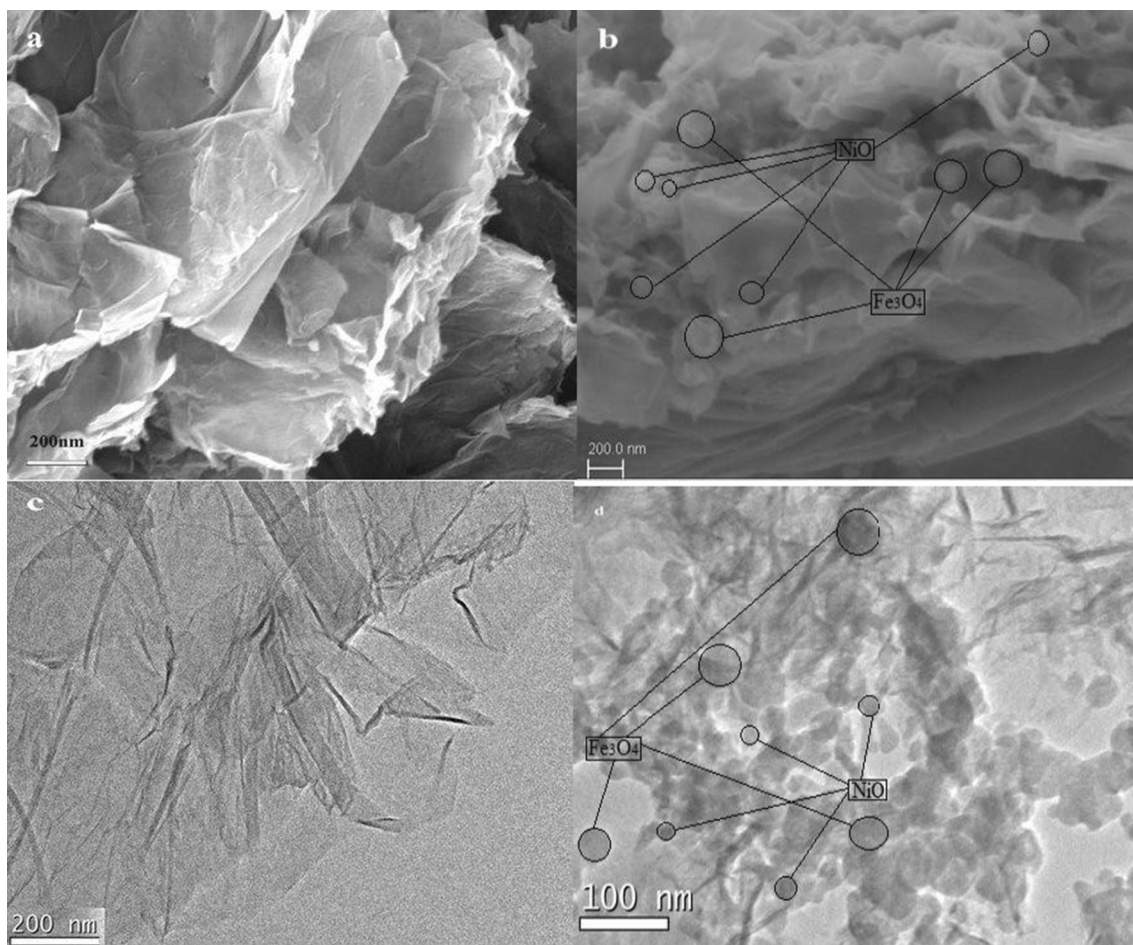
Fig. 3 The SEM of GNs (**a**) and GNs/Fe$_3$O$_4$/NiO (**b**) nanocomposites, the TEM of GNs (**c**) and GNs/Fe$_3$O$_4$/NiO (**d**) nanocomposites
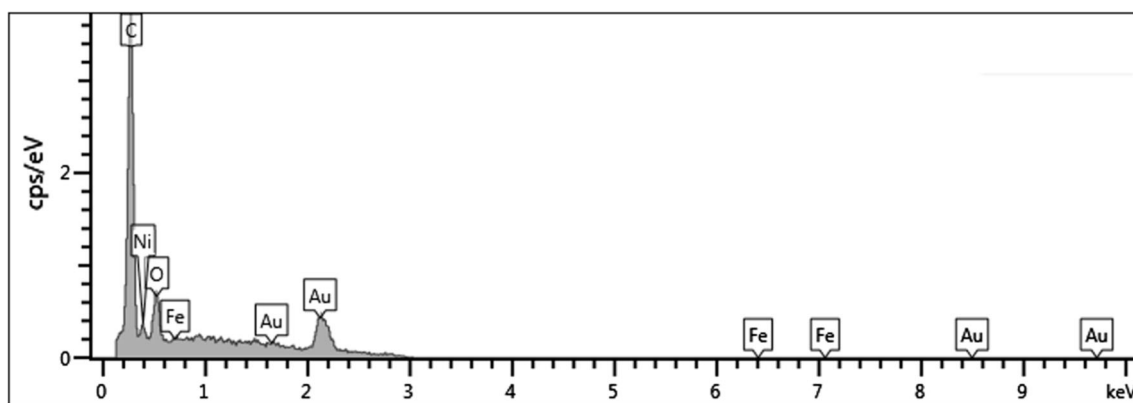

Fig. 4 EDX spectra of GNs/Fe$_3$O$_4$/NiO (S3) nanocomposites

had two times of quality loss in the test temperature range when the temperatures below 180 °C, quality loss is mainly causing by the volatile of water molecules, the quality loss between 180 and 300 °C, may be the thermal decomposition of containing oxygen groups of graphite oxide, the formation CO, CO_2, H_2O and so on. The TGA curves of GNs/Fe$_3$O$_4$/NiO nanocomposites shown in Fig. 5d, when the temperatures below 200 °C, quality loss is mainly causing by the volatile of water molecules the quality loss between 200 and 300 °C, may be due to the most containing oxygen groups has been removed the GNs/Fe$_3$O$_4$/NiO has very good thermal stability. The thermal stability
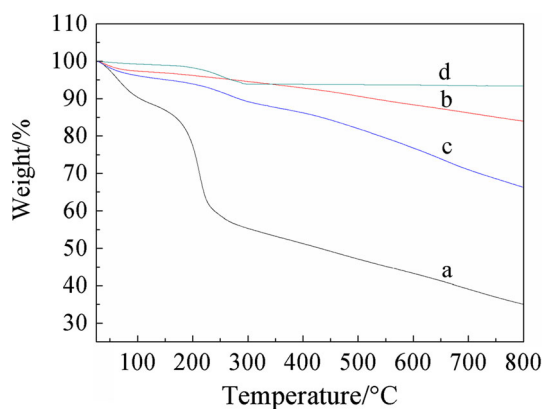
Fig. 5 The TGA curves of GO (*a*), GNs (*b*), GNs/Fe$_3$O$_4$ (*c*) and GNs/Fe$_3$O$_4$/NiO (*d*) nanocomposites

of NiO is higher, after combined NiO, the thermal stability of the nanocomposites material is significantly enhanced.

3.4 XRD analysis

The XRD patterns of GO, GNs, NiO, Fe$_3$O$_4$ MNPs and GNs/Fe$_3$O$_4$ nanocomposites are showed in Fig. 6. The diffraction peak of GO appears at around $2\theta = 11.8°$ obtained from the peak position, which indicates that the interlayer spacing is about ~ 0.85 nm calculated using Bragg's law ($\lambda = 2d \sin \theta$). However, this peak disappears in the XRD pattern of GNs and a new one arises at around $2\theta = 26.5°$, which corresponds to an interlayer spacing of ~ 0.94 nm. The reason for this is that the hydroxy and carboxyl groups of GO reacted with phenyl isocyanate, causing the anion electrostatic repulsion between the GO layers, thus resulting in an increase in the interlayer spacing. Figure 6c presents the XRD pattern of the NiO nanoparticles [39]. The characteristic peaks of NiO appear at $2\theta = 37.41°$, $43.36°$, $62.94°$ and $75.43°$, respectively.
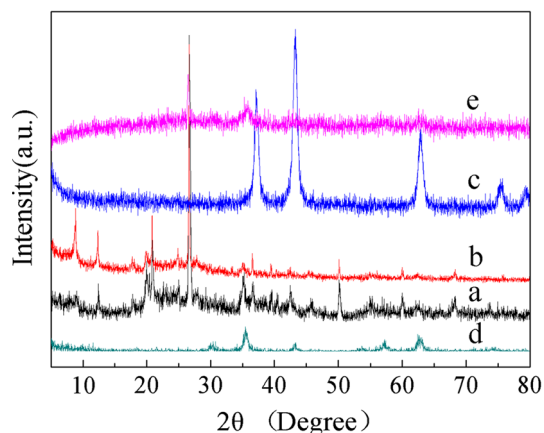
Figure 6d is the XRD pattern of the Fe$_3$O$_4$ nanoparticles. The locations of the diffraction peaks are consistent with the diffraction data of the bulk Fe$_3$O$_4$ with face-centered cubic structure. There are no obvious diffraction peaks of other phases, which indicate a high purity. XRD can be utilized to evaluate peak broadening with grain size and lattice strain due to dislocation [40]. Figure 6e shows the XRD patterns of GNs/Fe$_3$O$_4$ nanocomposite, there is no characteristic peak of GO ($2\theta = 11.8°$) or graphite ($2\theta = 24.5°$), suggesting that the graphene oxide was well reduced and the restacking of the as-reduced graphene sheets was effectively prevented [41].

3.5 Magnetic properties

To study the magnetic properties of the nanocomposites, the room-temperature magnetization hysteresis curves of the as-synthesized nanocomposites were measured using vibrating sample magnetometry (VSM), are shown in Fig. 7. All the as-made samples displayed typical ferromagnetic behaviour. The saturation magnetization of GNs/Fe$_3$O$_4$/NiO nanocomposites were about 22.42 (S3), 43.33 (S2) and 63.07 (S1) emu g^{-1}, respectively. The curve passed the original spot, which indicated super paramagnetism, a typical property of Fe$_3$O$_4$ [42]. That indicating the composite material has good magnetic properties, that can make the nanocomposites available recycle and reuse under plus magnetic field.

3.6 Photocatalytic performance of the nanocomposites

Figure 8 displays the adsorption and photocatalytic performance of the NiO, GNs/NiO and magnetic GNs/Fe$_3$O$_4$/NiO nanocomposites [43] with different mass ratio (NiO wt%, S1 = 50 wt%, S2 = 67 wt%, S3 = 75 wt%) to
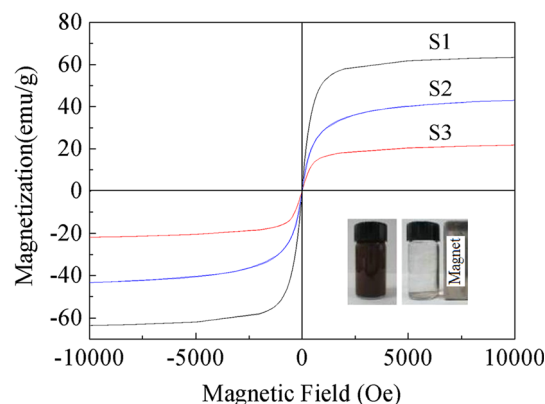

Fig. 6 The XRD patterns of GO (*a*), GNs (*b*), NiO MNPs (*c*), Fe$_3$O$_4$ MNPs (*d*) and GNs/Fe$_3$O$_4$ (*e*) nanocomposites

Fig. 7 The magnetization curves images of GNs/Fe$_3$O$_4$/NiO (*S1*, *S2*, *S3*) and magnetic separability of Fe$_3$O$_4$/NiO/GNs (*S3*) nanocomposites

p-nitrophenol (a) and rhodamine B (b). Herein, p-nitrophenol and rhodamine B ware selected as model organic pollutants to evaluate the photocatalytic activities of photocatalysts. Before the photocatalysis reaction, the adsorption equilibrium experiments were conducted firstly. After the adsorption reached equilibrium, the lamp (100 W mercury lamp) was switched on, and the photocatalysis reaction began. The photolysis of p-nitrophenol and rhodamine B aqueous solution ware analyzed comparing with the photocatalysts.

After 20 min of adsorption equilibrium, the adsorption rate of each sample (NiO, GNs/NiO, GNs/Fe$_3$O$_4$/NiO (S1, S2, S3) to p-nitrophenol were 1.5, 3.3, 3.1, 3.0, 2.8 %; and the adsorption rate of each sample (NiO, GNs/NiO, GNs/Fe$_3$O$_4$/NiO (S1, S2, S3) to rhodamine B were 2.1, 3.8, 3.5, 3.3, 3.1 %. The adsorption rate is proportional to the content of graphene in each sample. The results showed that photocatalytic degradation rate of magnetic GNs/Fe$_3$O$_4$/NiO nanocomposites (S3) with 75 % to p-nitrophenol and rhodamine B were 94.1 and 86.7 % after 2 h, respectively. The photocatalytic activity increased when the content of NiO NPs increased from 50 to 75 wt%. On the other hand, adsorption ability of GNs/NiO and GNs/

Fe$_3$O$_4$/NiO nanocomposite increased obviously comparing with pure NiO. Since the magnetic responsiveness of GNs/Fe$_3$O$_4$/NiO (S3) nanocomposites is very strong, it is conducive to recycle and reuse, not only save the resources but also more practical in real life.

The UV–Vis absorption spectra [44] of p-nitrophenol (a) and rhodamine B (b) in the presence of GNs/Fe$_3$O$_4$/NiO (S3) under UV irradiation as shown in Fig. 9. With the increase of the illumination time, the concentration of p-nitrophenol and rhodamine B were reduced. The insert of Fig. 9a, b showed the change of the color and concentration of p-nitrophenol and rhodamine B after photocatalytic degradation at different times: 0, 60, and 120 min.

3.7 Reusability test of the photocatalyst

GNs/Fe$_3$O$_4$/NiO (S3) nanocomposites (75 wt%) was recovered and recycled after the experiment of testing its reusability, as shown in Fig. 10a, b. It can be seen that the degradation rate of GNs/Fe$_3$O$_4$/NiO nanocomposites for p-nitrophenol (a) and rhodamine B (b) remains more than
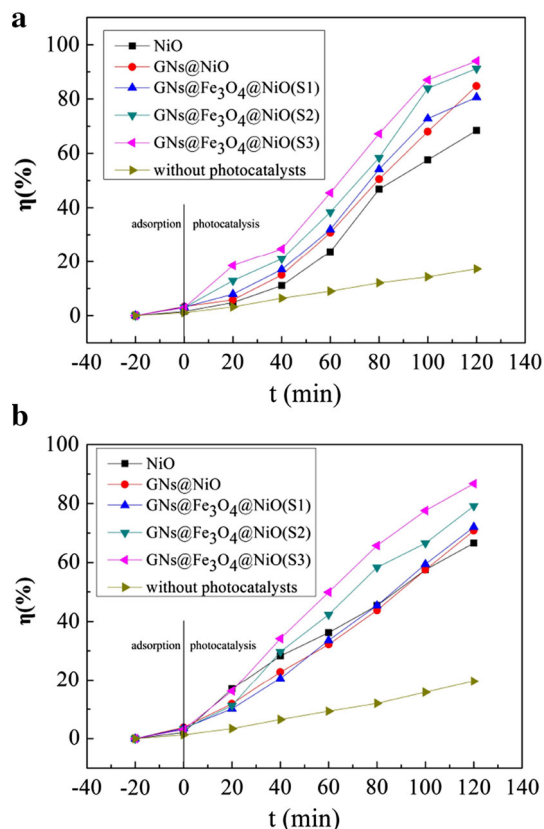

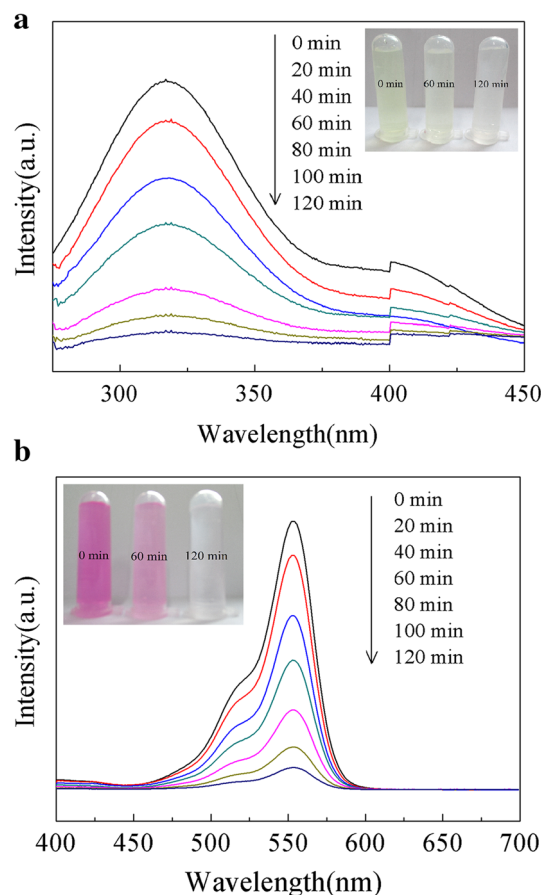Fig. 8 Photodegradation of p-nitrophenol (a) and rhodamine B (b) with different materials (NiO, GNs@NiO, GNs/Fe$_3$O$_4$/NiO)

Fig. 9 UV–Vis absorption spectra of p-nitrophenol (a) and rhodamine B (b) in the presence of GNs/Fe$_3$O$_4$/NiO (S3) under UV irradiation
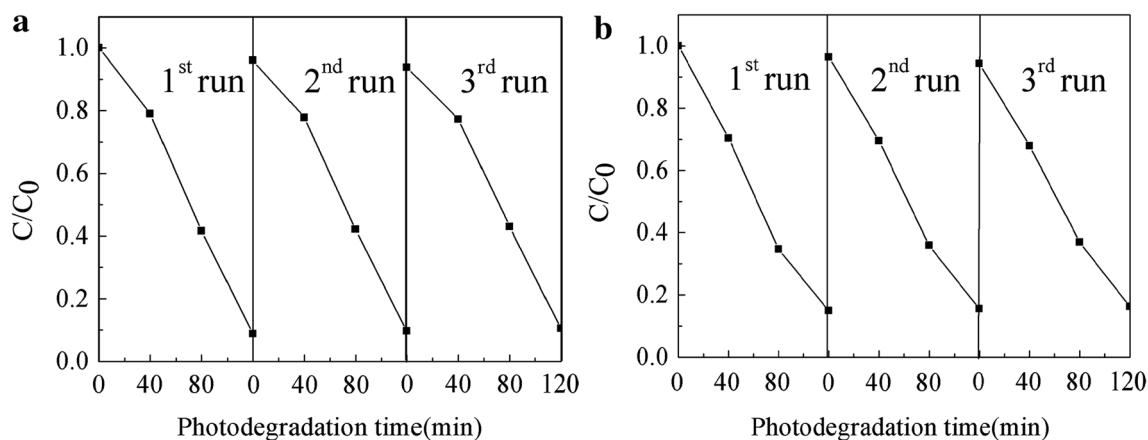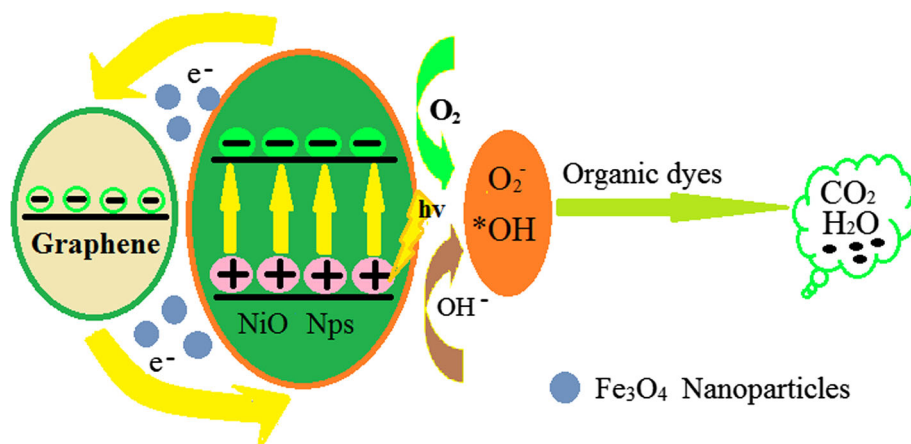
Fig. 10 The reusability of GNs/Fe$_3$O$_4$/NiO (S3) nanocomposites to degrade the p-nitrophenol (**a**) and rhodamine B (**b**)

Fig. 11 The simplified mechanism for the enhanced photocatalytic activity of GNs/Fe$_3$O$_4$/NiO nanocomposites

90.0 and 84.0 % after three times of repeated use. Therefore, the photocatalytic activity of GNs/Fe$_3$O$_4$/NiO (S3) nanocomposites for p-nitrophenol (a) and rhodamine B (b) has no obvious decline and reveals good reusability.

3.8 Photocatalytic mechanism for enhanced photocatalytic activity of GNs/Fe$_3$O$_4$/NiO nanocomposites

As shown in Figs. 8 and 10, GNs/Fe$_3$O$_4$/NiO nanocomposites exhibits both well photocatalytic activity and reusability. Figure 11 is the simply mechanism for enhanced photocatalytic activity of GNs/Fe$_3$O$_4$/NiO nanocomposites. It was found that graphene can store a large number of electrons and transport these electrons. When NiO Nps coated on graphene, it promoted the transfer of the electrons onto graphene surface Fe$_3$O$_4$ has excellent electrical conductivity and the electrostatic attraction between oxygen-containing groups and cationic dye can also promoted the transfer of the electrons. On the other hand, the particle size and specific surface area may effect the photocatalytic ability and adsorption ability. The larger surface area of

graphene can inhibit the growth of NiO Nps, and make reunion phenomenon reduced, which result in the sizes of NiO Nps smaller. The specific surface area and activity can be increased as the size of NiO Nps decreasing. When the specific surface area increased, the adsorption ability of materials increased. The excellent adsorption ability can increase the contact chance of contaminant molecules and materials, which enhanced the photodegradation rate. Therefore, the photocatalytic activity has been remarkably improved, due to the synergy effect between adsorption and photodegradation. Through the obtained removal efficiency, it also can be considered that photocatalytic degradation makes a considerable contribution to remove organic pollutants from wastewater.

4 Conclusion

In summary, we designed a facile route to synthesize magnetic photocatalyst GNs/Fe$_3$O$_4$/NiO nanocomposites successfully. Due to the nanocomposites has good photocatalytic performance, it can photocatalytic degrade p-nitrophenol and

rhodamine B in wastewater. The results indicated that the content of NiO has significant effect on the photocatalytic performance of GNs/Fe$_3$O$_4$/NiO. Besides the content of Fe$_3$O$_4$ has significant effect on the magnetic absorbing performance of GNs/Fe$_3$O$_4$/NiO nanocomposites. The saturation magnetization of GNs/Fe$_3$O$_4$/NiO (S3) nanocomposites was about 22.42 emu g^{-1}, and it has high photocatalytic efficiency to p-nitrophenol and rhodamine B. Furthermore, the photocatalytic degradation rate of GNs/Fe$_3$O$_4$/NiO (S3) nanocomposites to p-nitrophenol and rhodamine B were about 94.1 and 86.7 %, respectively. After three times of repeated use, the degradation rate of GNs/Fe$_3$O$_4$/NiO (S3) nanocomposites for p-nitrophenol (a) and rhodamine B (b) remains more than 90 and 84 %, which indicated the nanocomposites has good photocatalytic performance and a great potential application in the field of photocatalysis in the future.

References

1. L.L. Ma, H.Z. Sun, Y.G. Zhang, L.L. Yu, J.L. Li, E.K. Wang, Y. Yu, M. Tan, J.B. Wang, Nanotechnology **19**, 115709 (2008)
2. R. Asahi, T. Morikawa, T. Ohwaki, K. Aoki, Y. Taga, Science **293**, 269 (2001)
3. Z. Zou, J. Ye, K. Sayama, H. Arakawa, Nature **414**, 625 (2001)
4. K. Maeda, K. Teramura, D. Lu, T. Takata, N. Saito, Y. Inoue, K. Domen, Nature **440**, 295 (2006)
5. R.M. Trommer, A.K. Alves, C.P. Bergmann, J. Alloys Compd. **491**, 296–300 (2010)
6. G. Liu, G.S. Li, X.Q. Qiu, L.P. Li, J. Alloys Compd. **481**, 492–497 (2009)
7. X.W. Zeng, Y.X. Gan, E. Clark, L.S. Su, J. Alloys Compd. **509**, L221–L227 (2011)
8. Y. Zhao, C.Z. Li, X.H. Liu, F. Gu, J. Alloys Compd. **440**, 281–286 (2007)
9. D.H. Pieper, V.A.P. Martins dos Santos, P.N. Golyshin, Curr. Opin. Biotechnol. **15**, 215–224 (2004)
10. Z. Aksu, E. Kabasakal, Sep. Purif. Technol. **35**, 223–240 (2004)
11. A. Legrouri, M. Lakraimi, A. Barroug, A. De Roy, J.P. Besse, Water Res. **39**, 3441–3448 (2005)
12. W.K. Lafi, Z. Al-Qodah, J. Hazard. Mater. **137**, 489–497 (2006)
13. J.M. Herrmann, C. Duchamp, M. Karkmaz, B.T. Hoai, H. Lachheb, E. Puzenat, C. Guillard, J. Hazard. Mater. **146**, 624–629 (2007)
14. C.Y. Kwan, W. Chu, Water Res. **37**, 4405–4412 (2003)
15. E.I. Seck, J.M. Dona-Rodríguez, C. Fernández-Rodríguez, O.M. González-Díaz, J. Arana, J. Pérez-Peña, Appl. Catal. B **125**, 28–34 (2012)
16. R.D. Ambashta, M. Sillanpää, J. Hazard. Mater. **180**, 38–49 (2010)
17. W.X. Zhang, J.C. Cui, C.A. Tao, Y.G. Wu, Z.P. Li, L. Ma, Y.Q. Wen, G.T. Li, Angew. Chem. Int. Ed. **48**, 5864 (2009)
18. D. Li, M.B. Muller, S. Gilje, R.B. Kaner, G.G. Wallace, Nat. Nanotechnol. **3**, 101 (2008)
19. Y.X. Huang, X.W. Liu, J.F. Xie, G.P. Sheng, G.Y. Wang, Y.Y. Zhang, A.W. Xu, H.Q. Yu, Chem. Commun. **47**, 5795 (2011)
20. K.S. Novoselov, A.K. Geim, S.V. Morozov, D. Jiang, Y. Zhang, S.V. Dubonos, I.V. Grigorieva, A.A. Firsov, Science **306**, 666–669 (2004)
21. D.A. Dikin, S. Stankovich, E.J. Zimney, R.D. Piner, G.H.B. Dommett, G. Evmenenko, S.T. Nguyen, R.S. Ruoff, Nature **448**, 457–460 (2007)
22. Y. Xu, H. Bai, G. Lu, C. Li, G. Shi, J. Am. Chem. Soc. **130**, 5856–5857 (2008)
23. Y.H. Lu, W. Chen, Y.P. Feng, J. Phys. Chem. B **113**, 2–5 (2009)
24. H. Zhang, X. Lv, Y. Li, Y. Wang, J. Li, ACS Nano **4**, 380–386 (2010)
25. T.N. Lambert, C.A. Chavez, B. Hernandez-Sanchez, P. Lu, N.S. Bell, A. Ambrosini, T. Friedman, T.J. Boyle, D.R. Wheeler, D.L. Huber, J. Phys. Chem. C **113**, 19812–19823 (2009)
26. Y. Zhang, Z. Tang, X. Fu, Y. Xu, ACS Nano **4**(12), 7303–7314 (2010)
27. Y. Lin, Z. Geng, H. Cai, L. Ma, J. Chen, J. Zeng, N. Pan, X. Wang, Eur. J. Inorg. Chem. **2012**, 4439–4444 (2012)
28. Y.H. Chen, L.L. Chen, N.C. Shang, J. Hazard. Mater. **172**(1), 20–29 (2009)
29. Y.H. Chen, Y.Y. Liu, R.H. Lin, F.S. Yen, J. Hazard. Mater. **163**(2-3), 973–981 (2009)
30. X.D. Huang, X.F. Zhou, K. Qian, D.Y. Zhao, Z.P. Liu, C.Z. Yu, J. Alloys Compd. **514**, 76–80 (2012)
31. C. Zhang, Z.L. Mo, P. Zhang et al., Mater. Lett. **106**, 107–110 (2013)
32. J.P. Zhao, S.F. Pei, W.C. Ren, L.B. Gao, H.M. Cheng, ACS Nano **4**, 5245–5252 (2010)
33. Z. Xu, C. Shen, Y. Hou, H. Gao, S. Sun, Chem. Mater. **21**, 1778–1780 (2009)
34. Y.C. Dong, R.G. Ma, M.J. Hu, H. Cheng, C.K. Tsang, Q.D. Yang, Y.Y. Li, J.A. Zapien, J. Solid State Chem. **201**, 330–337 (2013)
35. T.L. Lai, Y.Y. Shu, G.L. Huang, C.C. Lee, C.B. Wang, J. Alloy. Compd. **450**, 318–322 (2008)
36. Y.X. Xu, H. Bai, G.W. Lu, C. Li, G.Q. Shi, J. Am. Chem. Soc. **130**, 5856 (2008)
37. J. Ge, Y. Hu, M. Biasini, W.P. Beyermann, Y. Yin, Angew. Chem. Int. Ed. **46**, 4342–4345 (2007)
38. A. Lerf, H.Y. He, M. Forster et al., J. Phys. Chem. B **102**, 4477–4482 (1998)
39. D.D. Zhao, M.W. Xu, W.J. Zhou, J. Zhang, H.L. Li, Electrochim. Acta **53**, 2699–2705 (2008)
40. R. Yogamalar, R. Srinivasan, A. Vinu, K. Arigab, A.C. Bosea, Soild State Commun. **149**, 1919–1923 (2009)
41. M. Sathish, T. Tomai, I. Honma, J. Power Sources **217**, 85–91 (2012)
42. J. Qiu, M. Gu, Appl. Surf. Sci. **252**, 888–892 (2005)
43. R. Sellappan, J.F. Zhu, H. Fredriksson, R.S. Martins, M. Zäch, D. Chakarov, J. Mol. Catal. A Chem. **335**, 136–144 (2011)
44. J.H. Pan, X.S. Zhao, W.I. Lee, Chem. Eng. J. **170**, 363–380 (2011)